Nearly ideal spin tunneling efficiency in Fe/Mg/MgO/SiO$_x$/n^+-Si(001) junctions

Ryosho Nakane,[1,2,*] Mitsuki Ichihara,[1] Shoichi Sato,[1] and Masaaki Tanaka[1,3,†]

[1]*Department of Electrical Engineering and Information Systems, The University of Tokyo, 7-3-1 Hongo, Bunkyo-ku, Tokyo 113-8656, Japan*

[2]*Institute for Innovation in International Engineering Education, The University of Tokyo, 7-3-1 Hongo, Bunkyo-ku, Tokyo 113-8656, Japan*

[3]*Center for Spintronics Research Network (CSRN), The University of Tokyo, 7-3-1 Hongo, Bunkyo-ku, Tokyo 113-8656, Japan*

(Received 8 May 2018; published 28 February 2019)

We achieved nearly ideal spin tunneling efficiency η by lowering the interface trap density D_{it} with a SiO$_x$ insertion layer in Fe/Mg/amorphous-MgO(1.0–1.5 nm)/plasma-oxidized SiO$_x$ ($\sim$0.2 nm)/n^+-Si(001) junctions. The spin polarization P_S of tunneling electrons was estimated from three-terminal Hanle signals at 4 K. At the optimum MgO thickness and oxidation time, we obtained P_S which is nearly equal to the spin polarization P_{FM} of Fe at the Fermi level, that is, $\eta = P_S/P_{FM} = 0.93$. By quantitatively estimating D_{it} and P_S of various junctions, we show that lowering D_{it} is crucial to obtain $\eta \cong 1$.

DOI: 10.1103/PhysRevMaterials.3.024411

I. INTRODUCTION

To realize Si-based spin-functional electronic devices [1–3], the spin injection/extraction into/from Si through a ferromagnetic junction has been extensively studied [4–11]. For spin injectors/extractors, ferromagnetic metal (FM) electrode layers are widely used since electrons transported through a FM layer are spin polarized due to the spin polarization P_{FM} of the FM at the Fermi level.

Like in magnetic tunnel junctions, if there is a spin filter effect in a (001)-oriented FM/MgO/semiconductor junction, the spin polarization P_S of tunneling electrons can be significantly larger than P_{FM}. Although some works have attempted to achieve it, making P_S higher than P_{FM} or clear proof of the spin filter effect has not been reported [12,13]. In the studies on FM/MgO/Si tunnel junctions, P_S in Si was found to be significantly smaller than P_{FM} [7,9,10], although the theories [14,15] predicted that the resistance-area product (RA) of these junctions is large enough to realize $Ps \approx P_{FM}$. Thus, to establish the understanding and technology of the spin injector/extractor on Si, it is necessary to clarify how the spin injection/extraction is affected by microscopic electrical and magnetic imperfections originating from structural defects and/or interface states in the junctions [13], excluding the spin filter effect. For this purpose, an investigation utilizing FM/amorphous-insulator/Si junctions is needed and its ultimate goal is the spin tunneling efficiency $\eta = P_S/P_{FM} = 1$. Hereafter, we use $P_{FM} = P_{Fe} = 44\%$ [16] for a Fe layer to define η. Recently, we theoretically presented a "dead-layer model" [17] and experimentally verified it by using Fe/Mg/amorphous-MgO/Si junctions [10] and Fe/Mg/amorphous-SiO$_x$N$_y$/Si junctions [11], and we found that the suppression of a magnetically dead layer by inserting an ultrathin Mg layer is important to realize a high P_S. In such junctions, we obtained $\eta = 0.41$ at 4 K [10], but this η value was not high enough. On the other hand, since the interface traps at the insulator/Si interface can be spin scattering centers, lowering the interface trap density D_{it} is required to enhance η, as suggested in our previous report [11]. So far, researchers have investigated spin injection/extraction signals into/from n^+-Si using FM/SiO$_2$ tunnel barrier/Si junctions or similar junctions with a SiO$_2$ insertion layer between a tunnel barrier and Si, aiming at lowering D_{it} to realize high η [18]. Here, we report on systematic and quantitative investigations of the relation between spin injection/extraction signals and D_{it}.

The purpose of this study is to achieve much higher η by lowering D_{it} at the insulator/Si interface with a SiO$_x$ insertion layer. In particular, we quantitatively show how D_{it} at the MgO/Si interface affects P_S in Fe/Mg/amorphous-MgO/Si junctions with and without a SiO$_x$ layer between MgO and Si. We find that lowering D_{it} by inserting a SiO$_x$ layer is very effective to enhance P_S, and we achieve $P_S = 41\%$ which corresponds to $\eta = 0.93$ (close to 1).

II. SAMPLE PREPERATION AND CHARACTERIZATION

A. Sample structure and preparation

All the layered structures examined in this study are illustrated in Fig. 1(a), where the name for each structure will be used throughout this study. The preparation method of them was basically the same as that in our previous report [10], in which all the layers were deposited at room temperature after the thermal cleaning of the Si(001) substrate in an ultrahigh vaccum. To prepare a SiO$_x$ layer between MgO and Si in type-II, -IV, and -VI structures, we used plasma oxidation of a MgO/Si structure as shown in Fig. 1(b), in which the substrate temperature was room temperature, oxidation time t_{ox} was 1 or 3 min, and the radio frequency (rf) power and O$_2$ pressure were 100 W and 2×10^{-3} Pa, respectively. This technique is basically the same as that in Ref. [19] and it has the following advantages: (i) Oxidation can be performed at room temperature that is low enough to suppress the reaction of the MgO layer and Si substrate, and (ii) the

*nakane@cryst.t.u-tokyo.ac.jp
†masaaki@ee.t.u-tokyo.ac.jp

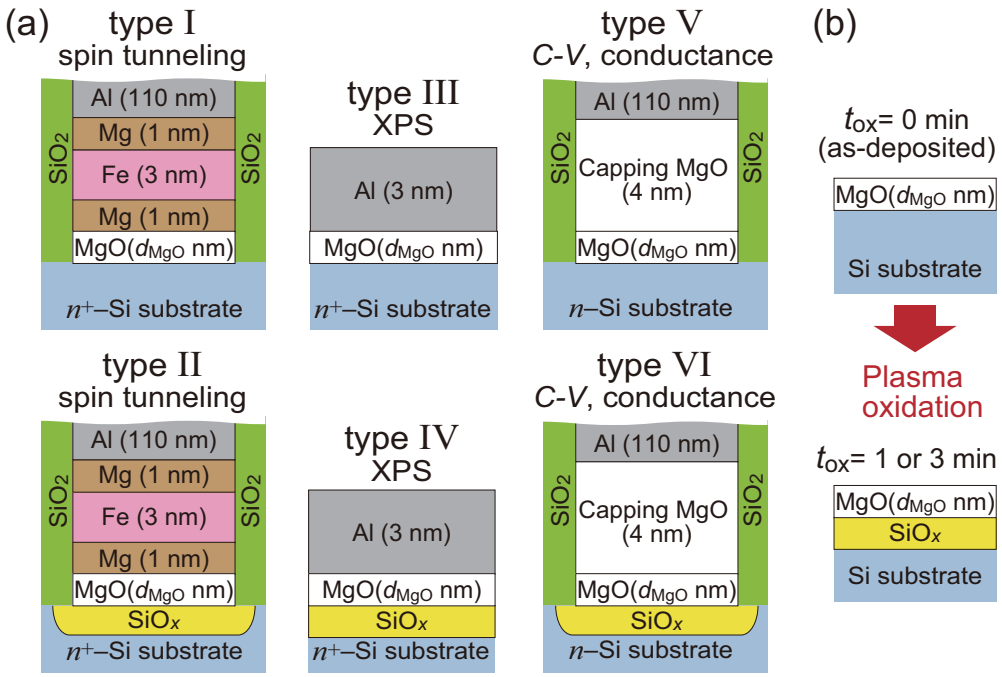

FIG. 1. (a) Layered structures examined in this study, where the name for each structure will be used throughout this study: Type I and II for spin tunneling measurements, type III and IV for x-ray photoelectron spectroscopy (XPS), and type V and VI for *C-V* and conductance measurements. (b) Formation procedure of SiO_x (yellow layer) inserted between a MgO layer and a Si substrate, where the as-deposited MgO/Si structure ($t_{ox} = 0$ min) is oxidized by O_2 plasma at room temperature for $t_{ox} = 1$ or 3 min.

amorphous-MgO layer is not crystallized during the oxidation process because of the low substrate temperature. We also prepared layered structures without plasma oxidation [type-I, -III, and -V structures in Fig. 1(a)] and, hereafter, these unoxidized structures are denoted by $t_{ox} = 0$ min. The phosphorus donor doping concentrations N_D in the n^+-Si(001) and n-Si(001) substrates were 8×10^{19} and 8×10^{16} cm^{-3}, respectively. For type-I, -II, -V, and -VI structures, we used a SiO_2/Si substrate, etched the surface SiO_2 layer, and opened circular areas (with 5.6–178 μm in diameter) of the Si surface, on which we formed junctions or capacitors whose shapes are cylindrical pillars surrounded by SiO_2 sidewalls for isolation, as shown in Fig. 1(a). In type-I and -II structures for spin tunneling measurements, a 1-nm-thick Mg layer was inserted between the Fe and MgO layers to suppress the formation of a magnetically dead layer [10,11].

B. Characterization of ferromagnetic tunnel junctions by x-ray photoelectron spectroscopy (XPS)

To characterize the SiO_x layer formed between MgO and Si by x-ray photoelectron spectroscopy (XPS), we prepared an unprocessed Al(3nm)/MgO(1.0 nm)/SiO_x/n^+-Si(001) structure with $t_{ox} = 0$ (type III) and 1 min (type IV). In the XPS measurements, an Al Kα x-ray source is used, the electron take-off angle (TOA), which is defined by the angle between the detector and substrate normal direction, as shown in Fig. 2(a), is $0 - 80^\circ$ and the electron pass energy (PE) of the analyzer is set at 15 eV. Figure 2(b) shows XPS spectra of Si $2p$ in the samples with $t_{ox} = 0$ and 1 min, which were measured at TOA $= 60^\circ$. In the analysis, we subtracted the background signal by the Shierly method, and then fitted Vogit functions to the experimental signals under the condition of the relative binding-energy (BE) differences derived from Ref. [20]; the peak BE positions of $Si^0{}_{1/2}$, Si^{1+}, Si^{2+}, Si^{3+}, and Si^{4+} are +0.6, +0.95, +1.75, +2.48, and +3.90 eV, respectively, from the peak BE position of $Si^0{}_{3/2}$. In Fig. 2(b), whereas there is no obvious peak from the Si^{2+} to Si^{4+} BE positions in the spectrum of the sample with $t_{ox} = 0$ min, a peak at around the Si^{4+} position appears in the spectrum of the sample with $t_{ox} = 1$ min.

To characterize the change in the material properties by the oxidaiton, XPS spectra of Mg $2p$ and $2s$ were also measured for Al(3nm)/MgO(1.0 nm)/SiO_x/n^+-Si(001) structures with $t_{ox} = 0$ (type III) and 1 min (type IV), where PE was set at 50 eV. In the analysis, we subtracted the background signal by the Shierly method and then fitted a Vogit function. Figures 2(c) and 2(d) show XPS spectra of the Mg $2p$ and $2s$ peaks measured with a take-off angle TOA $= 60^\circ$, respectively, where black and blue curves are the experimental results for $t_{ox} = 0$ and 1 min, respectively, and orange curves are the fitting curves. As shown in Fig. 2(d), in both samples, the Al KLL Auger peak with the peak BE position at ~90.5 eV is superimposed on the Mg $2p$ peak with the peak BE position at ~88 eV. Furthermore, the spectra of Al $2p$ in both samples have a metal Al peak (not shown), indicating that the MgO layer was not directly exposed to air because it was fully covered by the Al cap layer, while the samples were carried to the XPS equipment. Since the BE axis was not calibrated, we evaluated the XPS spectra of Mg $2p$ and $2s$ by the binding-energy difference Δ_{BE} between the peak BE positions; the Δ_{BE} in the samples with $t_{ox} = 0$ and 1 min are 37.00 and 36.62 eV, respectively, which are almost the same. Moreover, no additional peak appears by the oxidation. Thus, the prop-

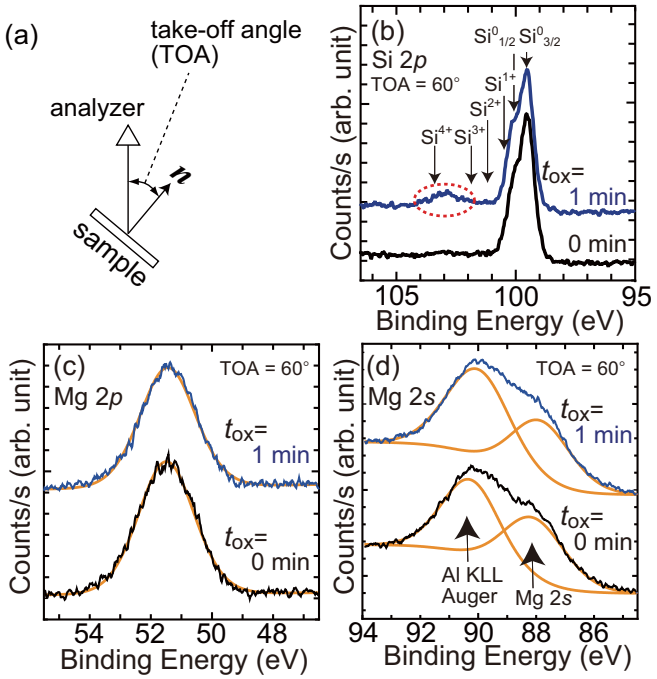

FIG. 2. (a) Definition of the take-off angle (TOA) in x-ray photoelectron spectroscopy (XPS) measurements, where $\boldsymbol{n}$ denotes the direction normal to the sample plane and the white arrow denotes the direction toward the analyzer. (b) X-ray photoelectron spectroscopy (XPS) spectra of Si $2p$ measured at TOA $= 60°$, where black and blue curves are the spectra of the Al(3 nm)/MgO(1 nm)/Si ($t_{ox} =$ 0 min, type III) and Al(3 nm)/MgO(1 nm)/SiO_x/Si ($t_{ox} = 1$ min, type IV), respectively. The binding-energy (BE) positions of $Si^0{}_{3/2}$, $Si^0{}_{1/2}$, Si^{1+}, Si^{2+}, Si^{3+}, and Si^{4+} are indicated by arrows. The peak marked by a red circle originates from SiO_x. (c),(d) XPS spectra of (c) Mg $2p$ and (d) Mg $2s$ measured at TOA $= 60°$, where black and blue curves are the experimental spectra of the Al(3 nm)/MgO(1 nm)/Si (oxidation time $t_{ox} = 0$ min, type III) and Al(3 nm)/MgO(1 nm)/SiO_x/Si ($t_{ox} = 1$ min, type IV), respectively, and orange curves are the fitting curves.

erties of the MgO layer were almost unchanged by the oxidation. In Fig. 2(b), the spectrum of the sample with $t_{ox} = 0$ min does not have any peak from the Si^{2+} to Si^{4+} BE positions, indicating that the MgO layer does not react with the Si substrate, and thus there are no silicate or silicide alloys formed at the MgO/Si interface. Considering the spectra of Si $2p$, Mg $2s$, and Mg $2p$, we concluded that the appearance of the peak at ~103 eV in the sample with $t_{ox} = 1$ min shown in Fig. 2(b) by the oxidation means the formation of SiO_x at the MgO/Si interface.

All of our XPS results revealed that there is no SiO_x at the MgO/Si interface without plasma oxidization ($t_{ox} = 0$ min), and that $SiO_x(x\sim2)$ was formed at the MgO/Si interface by the plasma oxidation for $t_{ox} = 1$ min. From angle-resolved XPS measurements of Si $2p$ with TOA $= 45°$–$70°$, the thickness d_{SiOx} of the SiO_x layer in the type-IV structure was estimated to be 0.26 nm from the peak area ratio of $(Si^0{}_{1/2} + Si^0{}_{3/2})/SiO_x$, assumming that the material parameters in SiO_x are the same as those in SiO_2 [21].

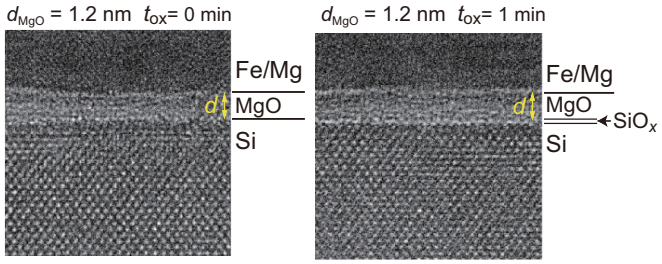

FIG. 3. Cross-sectional transmission electron microscopy (TEM) lattice images of (a) an Fe(3 nm)/Mg(1 nm)/amorphous-MgO($d_{MgO} = 1.2$ nm)/n^+-Si(001) junction ($t_{ox} = 0$ min, type I) and (b) an Fe(3 nm)/Mg(1 nm)/amorphous-MgO($d_{MgO} = 1.2$ nm)/SiO_x/n^+-Si(001) junction ($t_{ox} = 1$ min, type II), where the electron incidence is along the [110] axis of Si. The white layer corresponds to the MgO/SiO_x layer. The thickness d_{SiOx} of SiO_x was estimated to be 0.2 nm.

C. Characterization of ferromagnetic tunnel junctions by transmission electron microscopy (TEM) observation

We carried out cross-sectional transmission electron microscopy (TEM) observartion to check the heterointerfaces in the tunnel junction and to estimate the SiO_x thickness d_{SiOx}. Figures 3(a) and 3(b) show TEM lattice images of an Fe/Mg/amorphous-MgO($d_{MgO} = 1.2$ nm)/n^+-Si(001) junction ($t_{ox} = 0$ min, type I) and an Fe/Mg/amorphous-MgO($d_{MgO} = 1.2$ nm)/SiO_x/n^+-Si(001) junction ($t_{ox} =$ 1 min, type II), respectively, where the electron incidence is along the [110] axis of Si. The white layers in Figs. 3(a) and 3(b) correspond to the MgO and MgO/SiO_x layers, respectively. The interfaces on both sides of the white layer are smooth without visible void or crack and we estimated the thickness d of the white layer in each figure: Fig. 3(a) $d = 1.2$ nm and Fig. 3(b) $= 1.4$ nm. From the XPS reuslts, d_{SiOx} corresponds to the difference in d, and thus it was estimated to be 0.2 nm. In consequence, d_{SiOx} estimated by the TEM images is consistent with that (0.26 nm) estimated by the angle-resolved XPS spectra of Si $2p$.

III. SPIN POLARIZATION OF TUNNELING ELECTRONS

A. *I-V* characteristics of ferromagnetic tunnel junctions

For *I-V* and three-terminal Hanle measurements, we prepared vertical three-terminal devices having circular type-I and -II junctions with area $A = 25$, 250, 2500, and 25000 μm^2 on a n^+-Si(001) substrate: The layered structure of type I is (from top to bottom) Al(110 nm)/Mg(1 nm)/Fe(3 nm)/Mg(1 nm)/amorphous-MgO (thickness $d_{MgO} =$ 1.0, 1.2, and 1.5 nm)/n^+-Si(001), and that of type II is Al(110 nm)/Mg(1 nm)/Fe(3 nm)/Mg(1 nm)/amorphous-MgO($d_{MgO} = 1.0$, 1.2, and 1.5 nm)/SiO_x/n^+-Si(001). In the *I-V* characteristics of the junctions measured at room temperature and 4 K, nonlinear curves indicating tunnel current conduction were obtained for all the devices (not shown). For the same d_{MgO} and t_{ox}, the shape of the *I-V* curves and resistance-area product (*RA*) at room temperature were independent of *A*, meaning that leakage current is negligible in the junctions. Figure 4(a) shows *RA* at 0 V plotted as a function of t_{ox}, which were measured at 4 K for the devices

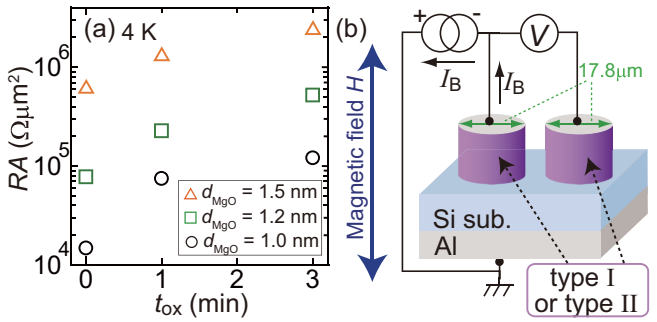

FIG. 4. (a) Resistance-area product (RA) at zero bias voltage of the junctions plotted as a function of t_{ox}, estimated from the I-V characteristics measured at 4 K. The open black circles, open green squares, and open orange triangles are the values for the MgO thickness $d_{MgO} = 1.0$, 1.2, and 1.5 nm, respectively. (b) Schematic illustration of a device having type-I (or type-II) structures with $A = 250\,\mu m^2$ (the diameter $= 17.8\,\mu$m) and the three-terminal Hanle measurement setup. Although a positive bias case ($I_B > 0$, spin injection geometry) is shown in the figure, we mainly use negative biases ($I_B < 0$, spin extraction geometry) in the present study. See, also, Fig. 6.

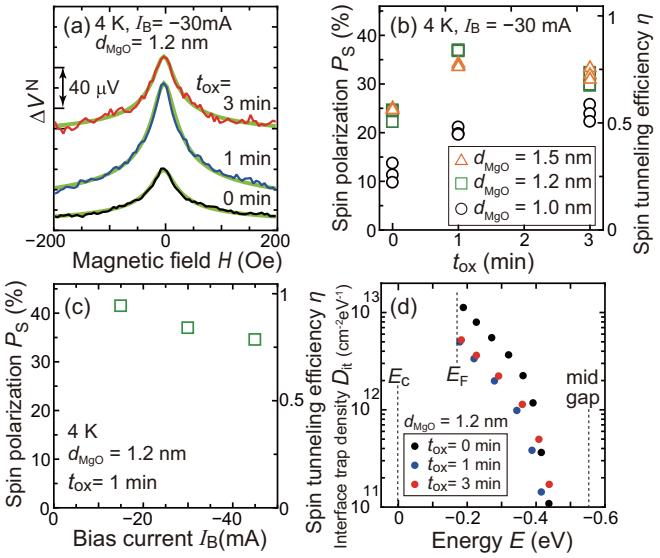

FIG. 5. (a) Narrower three-terminal Hanle signal ΔV^N of a device with $d_{MgO} = 1.2$ nm measured at 4 K with $I_B = -30$ mA (spin extraction geometry), where black, blue, and red curves are ΔV^N of the devices with $t_{ox} = 0$ (type I), 1, and 3 min (type II), respectively, and the light green curve superimposed on each ΔV^N is the fitting curve with Eq. (1). (b) Spin polarization P_S of tunneling electrons and spin tunneling efficiency η plotted as a function of t_{ox}, where each value was estimated form ΔV^N measured at 4 K with $I_B = -30$ mA. Open black circles, open green squares, and open orange triangles are the values for $d_{MgO} = 1.0$, 1.2, and 1.5 nm, respectively. (c) Bias current I_B dependence of P_S and η in the device with $d_{MgO} = 1.2$ nm and $t_{ox} = 1$ min (type II). (d) Interface trap density D_{it} in the capacitors with $d_{MgO} = 1.2$ nm and $t_{ox} = 0$ (type V), 1, and 3 min (type VI) as a function of electron energy E, where the origin of E is set at the conduction-band edge E_c of Si, the middle of the band gap of Si is indicated by "mid gap," and E_F denotes the Fermi level of the Si substrate. Black, blue, and red circles are D_{it} in the capacitors with $t_{ox} = 0$, 1, and 3 min, respectively.

with $A = 250\,\mu m^2$ (the diameter is 17.8 μm) and various d_{MgO}. From the exponential slope in the $RA - d_{MgO}$ plot (not shown), we estimated the barrier height of the MgO layer ($t_{ox} = 0$ min) for electrons to be 0.3 eV (which is the same as that in our previous study [10]). As shown in Fig. 4(a), RA increases with increaing t_{ox} for all the d_{MgO} cases, which indicates that d_{SiO_x} increases with increasing t_{ox}.

B. Measurement of Hanle signals and procedure for estimating the spin polarizarization P_S of tunneling electrons

Figure 4(b) shows the three-terminal Hanle measurement setup, in which the voltage change ΔV is measured with a constant current I_B, while a magnetic field H perpendicular to the substrate is applied and varied between ±3 kOe. In this study, we mainly use negative I_B, where electrons flow from the semiconductor to the ferromagnet (spin extraction geometry). To estimate P_S and τ_S, we use the following formula [10] of the narrower Hanle signal ΔV^N:

$$\Delta V^N(H) = \Delta V_0^N \sqrt{\frac{1+\sqrt{1+(\gamma\tau_S H)^2}}{2+2(\gamma\tau_S H)^2}}, \quad (1)$$

$$\Delta V_0^N = J\rho_s\lambda_S P_S^2, \quad (2)$$

where J is the current density defined by I_B/A, $\lambda_S = (D_e\tau_S)^{0.5}$ is the spin diffusion length in Si, D_e is the diffusion coefficient of electrons in Si, τ_S is the spin lifetime in Si, ρ_s is the resisitivity of Si, and γ is the gyromagnetic ratio. As demonstrated in our previous study [10], we can estimate accurate P_S and τ_S from ΔV^N using Eqs. (1) and (2) since our vertical device structure is free from the channel confinement effect which becomes more remarkable in lateral device structures with a thinner channel layer. The values of ρ_s and D_e at 4 K were estimated to be 0.6 mΩcm and 6.00 cm^2/s, respectively, by the van der Pauw method. Recent studies [6,10,11] have shown that the three-terminal signal ΔV consists of ΔV^N with a typical half width at half maximum (HWHM) of a few-tens Oe and the broader background signal with a typical HWHM of a few-hundred Oe. Since the latter broader signal is not related to spin injection or extraction signals [6,10], we focus on the former narrower signal in this study. The estimation procedure of ΔV^N is shown in the Supplemental Material [22].

C. Device parameters for nearly ideal P_S

To estimate P_S and τ_S, ΔV of our three-terminal devices with $A = 250\ \mu m^2$ was measured with $I_B = -30$ mA at 4 K. Since ΔV does not have hysteresis, we averaged signals for the external magnetic field with two sweeping directions (from positive to negative, and vice versa). To ensure the accuracy of estimation and to confirm the reproducibility, three devices with the same d_{MgO} and t_{ox} were measured. Figure 5(a) shows ΔV^N versus H of the devices with $d_{MgO} = 1.2$ nm, where the black, blue, and red curves are the experimental ΔV^N for $t_{ox} = 0$, 1, and 3 min, respectively, and the green curve on each experimental ΔV^N is the fitting curve with Eq. (1). We found that whereas P_S depends on t_{ox} [Fig. 5(b)], τ_S is

estimated to be ∼3.1 ns (2.5−3.6 ns) for all t_{ox}, which is comparable to the values reported previously [7–10], and this result is consistent with the theoretical prediction [23] and electron spin resonance (ESR) experiments [18] for the N_D value in this study. This fact supports the validity of our fitting procedure. Figure 5(b) shows P_S and η, where three values for the three devices with the same d_{MgO} and t_{ox} are very similar and thus reproducible. At the same t_{ox}, P_S for $d_{MgO} = 1.0$ nm is smaller than P_S for $d_{MgO} = 1.2$ and 1.5 nm, and it monotonically increases with increasing t_{ox}. On the other hand, as t_{ox} increases from 0, P_S for $d_{MgO} = 1.2$ and 1.5 nm increases and shows the maximum at $t_{ox} = 1$ min, and then slightly decreases at $t_{ox} = 3$ min. The maximum $P_S = 38\%$ ($\eta = 0.86$) was obtained for $d_{MgO} = 1.2$ nm with $t_{ox} = 1$ min. Interestingly, the $RA - t_{ox}$ relation in Fig. 4(a) does not correlate with the $P_S - t_{ox}$ relation in Fig. 5(b); RA for $d_{MgO} = 1.2$ and 1.5 nm monotonically increases with increasing t_{ox}, but P_S for those d_{MgO} has the peak at $t_{ox} = 1$ min. Thus, the enhancement of P_S is not simply explained by the increase of d_{SiOx} or d_{MgO}. We also investigated the I_B dependence of P_S for $d_{MgO} = 1.2$ nm with $t_{ox} = 1$ min, as shown in Fig. 5(c), and found that P_S monotonically increases with decreasing $|I_B|$ and that the highest $P_S = 41\%$ ($\eta = 0.93$) was obtained at $I_B = -15$ mA.

IV. INFLUENCE OF INTERFACE STATE DENSITY ON SPIN TUNNELING EFFICIENCY

To examine how D_{it} at the insulator/Si interface affects P_S using the conductance method [24], we prepared circular Al/MgO/n-Si (metal-oxide-semiconductor: MOS) capacitors with $A = 25000\,\mu m^2$ by the following process. After thermal cleaning of a phosphorus-doped n-Si(001) substrate having a heavily phouphrus-dopoed backside with $N_D \sim 10^{20}\,cm^{-3}$, a MgO layer with $d_{MgO} = 1.2$ nm was deposited onto the substrate surface and then it was oxidized at room temperature for $t_{ox} = 0$ (type V), 1, and 3 min (type VI). Subsequently, a 4-nm-thick MgO capping layer was deposited onto the previously deposited MgO layer and a 10-nm-thick Al layer was subsequently deposited. Finally, a 100-nm-thick circular Al pad was formed on the top and an Al layer was deposited on the backside of the substrate.

First, the surface potential ϕ_S of Si was estimated by a high-frequency capacitance-voltage (C-V) curve measured at 1 MHz [24], and then D_{it} was estimated by the conductance method (see the Supplemental Material [22]). These measurements were carried out at room temperature. Figure 5(d) shows D_{it} plotted as a function of electron energy E, where the maximum E for the data is E_F of the Si substrate, which is lower by 0.17 eV than the conduction-band edge E_C of Si since we used the conductance method in the dc voltage range where the surface of Si in the MOS capacitor is depleted. In the figure, D_{it} exponentially decreases with lowering E towards the middle of the band gap [denoted by "mid gap" in Fig. 5(d)] in all the cases, and each $D_{it} - E$ plot is almost parallel to each other. At any E, as t_{ox} increases from 0, D_{it} decreases at $t_{ox} = 1$ min, and then it slightly increases at $t_{ox} = 3$ min. Thus, this behavior highly correlates with the t_{ox} dependence of P_S for $d_{MgO} = 1.2$ nm in Fig. 5(b); the device with lower D_{it} shows higher P_S. Although D_{it} at around E_C cannot be estimated by the conductance method, it is reasonable that the relation of D_{it} and t_{ox} is maintained in the E range between E_F and E_C since D_{it} continiously changes with E and the $D_{it} - E$ plot for each t_{ox} is almost parallel to each other in Fig. 5(d). Thus, we concluded that the highest $P_S = 41\%$ ($\eta = 0.93$) in this study was achieved by lowering D_{it} at the insulator/Si interface.

V. DISCUSSION

In Sec. III, we estimated P_S using ρ_s measured by the van der Pauw method, the Hanle signals, Eqs. (1) and (2), and showed that P_S is nearly ideal (= 41%) for $d_{MgO} = 1.2$ nm with $t_{ox} = 1$ min. Since P_S is inversely proportional to $(\rho_s)^{0.5}$ in Eq. (2), the change in ρ_s changes P_S. Thus, the accurate estimation of P_S requires the accurate ρ_s value. Considering that Hanle signals originate from the accumulation of spin-polarized electrons near the surface of the Si channel, the accurate ρ_s value in this region is needed, although this has not been pointed out in this research field. From the basics of semiconductor physics, ρ_s near the Si surface is affected by the band bending of Si and the phosphorus donor concentration. Thus, there is a possibility that the ρ_s value estimated by the van der Pauw method is different near the surface of the Si channel. In this section, we estimate the ρ_s value near the Si surface in our devices by taking into account the band bending of Si and possible nonuniformity in the phosphorus donor doping concentration in the Si channel, and show that the P_S values in Figs. 5(b) and 5(c) are accurate.

A. Definition of forward and reverse bias ranges

In our definition, the bias range with the positive bias voltage $V_B(> 0)$ and current $I_B(> 0)$ corresponds to "the reverse bias range," and the bias range with the negative $V_B(< 0)$ and $I_B(< 0)$ corresponds to "the forward bias range," as shown in Fig. 6(a). The expressions "reverse" and "forward" come from the terminology in the research field of Schottky barriers and Schottky diodes [25]. (Note that our polarity definition in V_B and I_B here is opposite to the conventional polarity of Schottky diodes.) Our spin extraction signals were measured in the forward bias range ($V_B, I_B < 0$) for the Schottky barrier near the Si surface (electrons flow from the Si to the metal layers), as shown in Fig. 6(a). Figures 6(b)–6(d) show the band diagrams of our devices at various forward biases.

B. Estimation of the detailed electronic band profile of the Schottky barrier in our junction

The electrical properties of a Si substrate depend on the donor doping concentration N_D. In a ferromagnet/tunnel barrier/n^+-Si junction, there is a Schottky barrier in the n^+-Si substrate at zero bias ($V_B = 0$ V), as shown in Fig. 7(b). In the reverse bias range of the Schottky junction (when a positive V_B is applied; not shown in the figure), the band of n^+-Si near the tunnel barrier/n^+-Si interface bends further upward near the surface and the bending region is depleted. The depletion width W_D of the Schottky barrier depends on N_D and it can be estimated using the following "depletion approximation" in a metal-oxide-semiconductor (MOS) structure [26].

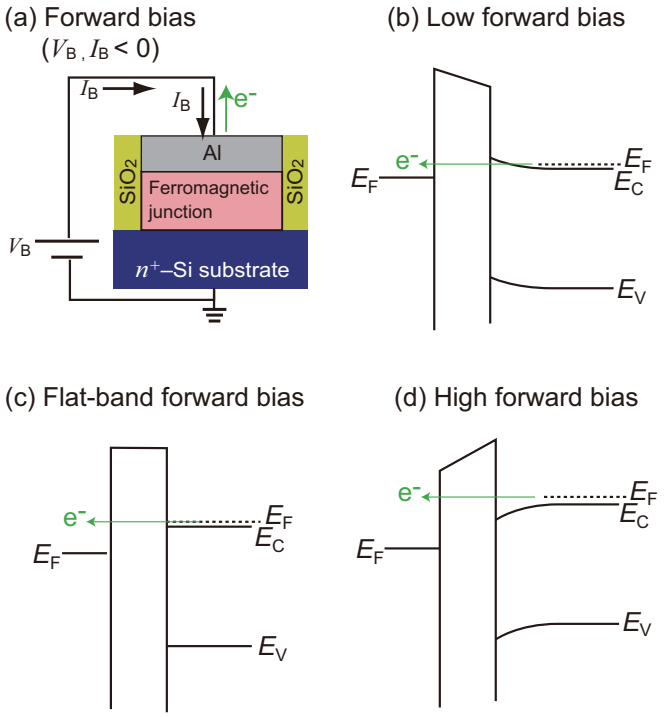

FIG. 6. (a) Definition of the bias polarity in this study. In our devices, the negative bias voltage V_B and the negative bias current I_B correspond to the "forward bias range," in which electrons flow from the n^+-Si to the metal layers. (b)–(d) Band diagrams of our devices. Direct-tunneling (DT) electron conduction via a Fe/Mg/MgO/n^+-Si junction in the forward bias range, where Si is degenerated: (b) DT via the Schottky barrier of Si and MgO layer in a forward bias with a magnitude smaller than $|V_{FB}|$, (c) DT via the MgO layer at the flat-band bias voltage $|V_{FB}|$, and (d) DT via the MgO layer in a forward bias with a magnitude larger than $|V_{FB}|$.

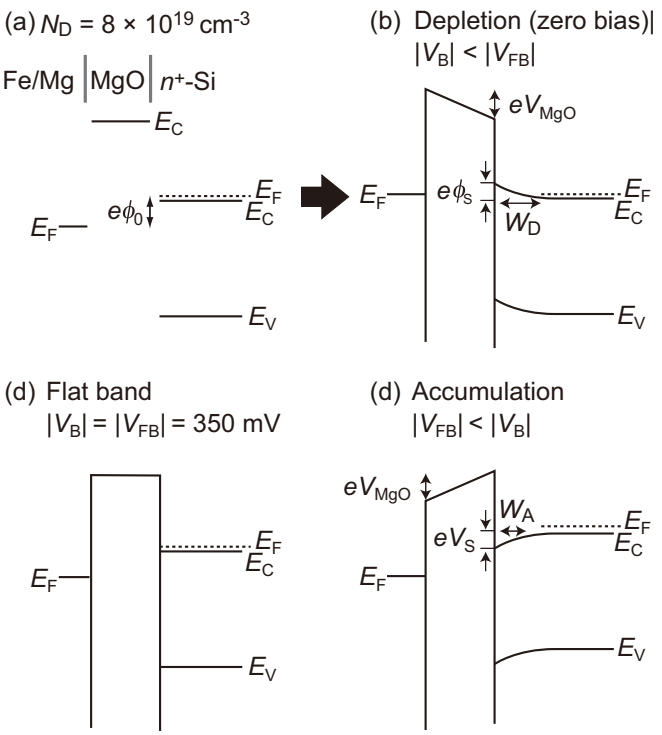

FIG. 7. (a)–(d) Energy band diagrams of a Fe/Mg/MgO/n^+-Si junction (degenerated Si with phosphorus donor doping concentration $N_D = 8 \times 10^{19}\,\mathrm{cm}^{-3}$), where E_C is the conduction-band minimum of Si or MgO, E_V is the valence-band maximum of Si, E_F is the Fermi energy, $e\phi_0$ is the difference in the work function between the Fe/Mg and Si, $e\phi_S$ is the band bending of Si at the Si surface in electron depletion, W_D is the depletion width in Si, eV_{MgO} is the energy drop in the MgO layer, eV_S is the band bending of Si at the Si surface in electron accumulation, W_A is the band-bending width of Si in electron accumulation, V_B is the bias voltage, and V_{FB} is the flat-band voltage ($V_{FB} < 0$ and $|V_{FB}| = 350\,\mathrm{mV}$). (a) Energy band diagram of each material before contact, (b) depletion of Si when $V_B = 0 < |V_{FB}|$, (c) flat-band of Si when $|V_B| = |V_{FB}| = 350\,\mathrm{mV}$ with $V_B < 0$, and (d) accumulation of Si when $|V_{FB}| < |V_B|$ with $V_B < 0$.

Here, we estimated W_D and the barrier height $e\phi_s$ (where e is the elementary charge) at zero bias voltage of the Schottky barrier [see Figs. 7(a) and 7(b)] using the following parameters; the difference in the work function $e\phi_0$ between the n^+-Si ($N_D = 8 \times 10^{19}\,\mathrm{cm}^{-3}$) and Fe/Mg is 350 meV, the MgO thickness d_{MgO} is 1.2 nm, the relative permittivity ε_{MgO} of MgO is 9.8, and the relative permittivity ε_{Si} of Si is 12. The $e\phi_0$ value (= 350 meV) was estimated from our previous paper with a Mg thickness of 1 nm [10]. The band-gap narrowing of n^+-Si was taken into account; the conduction-band bottom is lowered by ∼100 meV and the Fermi level is located ∼80 meV above the conduction-band bottom [27]. The electronic band profile of the junction at zero bias voltage is shown in Fig. 7(b).

The following equations are given in the depletion approximation:

$$\phi_0 = V_{MgO} + \phi_S, \tag{3}$$

$$\varepsilon_{MgO} F_{MgO} = \varepsilon_{Si} F_{Si}, \tag{4}$$

$$F_{si} = [(2eN_D\phi_S)/\varepsilon_0\varepsilon_{Si}]^{0.5}, \tag{5}$$

where V_{MgO} is the voltage drop in the MgO layer, $F_{MgO} = V_{MgO}/d_{MgO}$ is the electric field in the MgO layer, F_{Si} is the electric field at the surface of Si, and ε_0 is the vacuum permittivity. The following values were obtained in our three-terminal devices on the n^+-Si substrate ($N_D = 8 \times 10^{19}\,\mathrm{cm}^{-3}$) at zero bias ($V_B = 0\,\mathrm{V}$):

$$eV_{MgO} = 240\,\mathrm{meV}, \quad W_D = 1.3\,\mathrm{nm},$$
$$e\phi_S = 110\,\mathrm{meV}, \quad F_{Si} = 1.6\,\mathrm{MV/cm}.$$

From a simple estimation, the surface of Si is depleted for bias voltage $0 \leqslant |V_B| < 350\,\mathrm{mV}$, whereas it is flat for $|V_B| = \phi_0 = 350\,\mathrm{mV}$, as shown in Fig. 7(c). This bias voltage is called "the flat-band voltage V_{FB}", where $|V_{FB}| = 350\,\mathrm{meV}$ and $V_{FB} < 0$.

On the other hand, as shown in Fig. 7(d), in the forward bias range $|V_{FB}| < |V_B|$ with $V_B < 0$, the electronic band of n^+-Si near the tunnel barrier/Si interface slightly bends downward near the surface and electrons are accumulated in this case. However, estimating the detailed band bending is difficult unlike the case of the depletion approximation since it needs a self-consistent calculation which takes into account the Fermi-Dirac integral. Since the band bending

depends on N_D and F_{MgO}, we simply estimated the energy eV_S and width W_A of the band bending in Fig. 7(d) using Fig. 3 in Ref. [28], which is the relation between the band bending in Si and electric field in an oxide layer at 300 K. Here, we focus on $t_{MgO} = 1.2$ nm, $N_D = 8 \times 10^{19}$ cm^{-3}, and the bias voltages used in our three-terminal measurements. We assume $d_{MgO} = 1.3$ nm in the sample with $d_{MgO} = 1.2$ nm and $t_{ox} = 1$ min since the 0.26-nm-thick SiO_x is equivalent to a 0.1-nm-thick MgO layer in terms of relative permittivity. Note that the properties described here are almost the same as those at 4 K since the electrical properties of degenerated n^+-Si with $N_D = 8 \times 10^{19}$ cm^{-3} are temperature insensitive.

First, we describe an example of the estimation procedure for $d_{MgO} = 1.2$ nm and $t_{ox} = 0$ min, for $I_B = -30$ mA and $V_B = -620$ mV, which is the condition of Fig. 5(a). Using the flat-band voltage $|V_{FB}| = 350$ mV, the voltage drop of the total MgO/n^+-Si structure is 270 mV. Using the ε_{MgO} and ε_{Si} values, the electric field in the MgO layer F_{MgO} is $\sim$1.8 MV/cm, and the band bending of the Si surface V_S and the bending width W_A of Si were estimated to be 40 mV and 0.27 nm, respectively. The following values are obtained for $d_{MgO} = 1.2$ nm and $t_{ox} = 1$ min and various I_B in the same manner.

At $d_{MgO} = 1.2$ nm and $t_{ox} = 1$ min,

$I_B = -15$ mA, $F_{MgO} = 1.8$ MV/cm, $V_S = 30$ mV,

$W_A = 0.20$ nm;

$I_B = -30$ mA, $F_{MgO} = 3.0$ MV/cm, $V_S = 60$ mV,

$W_A = 0.28$ nm;

$I_B = -45$ mA, $F_{MgO} = 3.9$ MV/cm, $V_S = 110$ mV,

$W_A = 0.34$ nm.

We found that all the $|V_B|$ values used in the present study are higher than $|V_{FB}| = 350$ mV [the band diagram is shown in Fig. 7(d)], and that the maximum F_{MgO} in the three-terminal measurements is 3.9 MV/cm under the above-mentioned condition for $t_{MgO} = 1.2$ nm, $t_{ox} = 1$ min, and $I_B = -45$ mA, for which V_S and W_A are the maximum. For all the bias conditions, V_S and $W_A (= 0.2-0.34$ nm) values are much smaller than those in the depletion conditions, and thus the electronic band in the forward bias range ($V_B < 0, I_B < 0$) can be regarded as flat. Therefore, the electronic band bending of Si has little influence on the estimation of P_S in the spin extraction geometry we used in the present work. Even if there is a possibility that such electronic band bending affects the estimation of P_S, the P_S value ($= 41\%$) for $I_B = -15$ mA is the most reliable among all the conditions since $V_S (= 30$ mV) and $W_A (= 0.20$ nm) are the smallest (nearly flat-band condition).

C. Analysis of *I-V* characteristics and the donor doping concentration of the Si surface

Here, we analyze the electron conduction via the Schottky barrier in the Fe/Mg/MgO/n^+-Si (or Fe/Mg/MgO/SiO_x/n^+-Si) junctions with $d_{MgO} = 1.2$ nm and reveal that the doping concentration N_D' at the Si surface is larger than 6×10^{19} cm^{-3}, as described below, which is

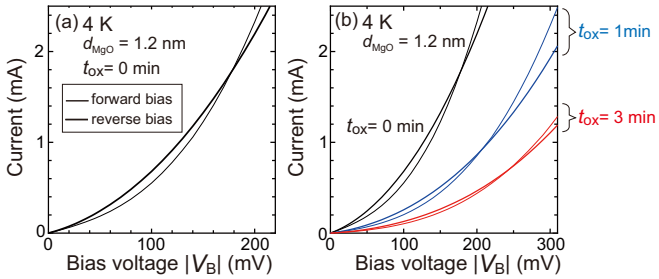

FIG. 8. (a) *I-V* characteristics measured at 4 K for the Fe/Mg/MgO/n^+-Si junction with $d_{MgO} = 1.2$ nm and $t_{ox} = 0$ min, where the thin and bold curves represent the *I-V* curves in the forward and reverse bias ranges, respectively. (b) *I-V* characteristics measured at 4 K for the Fe/Mg/MgO/n^+-Si junction with $d_{MgO} = 1.2$ nm and $t_{ox} = 0$ min (black curves), $t_{ox} = 1$ min (blue curves), and $t_{ox} = 3$ min (red curves), where the thin and bold curves represent the *I-V* curves in the forward and reverse bias ranges, respectively.

comparable to the N_D value of 8×10^{19} cm^{-3} estimated from the van der Pauw method. Then, we estimated the resistivity ρ_s (Ωcm) near the Si surface using the relation $\rho_s = 0.00055 \times (N_D')^{-2/3}$ obtained in the study of bulk Si materials [29]. If $N_D' = 6 \times 10^{19}$ cm^{-3}(this is the worst case), then P_S is overestimated and the calibrated spin polarization is $P_S \div 1.10$ using the increased ρ_s.

The electron conduction in our junction Fe/Mg/MgO/n^+-Si (or Fe/Mg/MgO/SiO_x/n^+-Si) is the direct tunneling through the barrier composed of the MgO layer (or the MgO/SiO_x bilayer) and the Schottky barrier of n^+-Si, as shown in Fig. 6(b), when $V_B < 0$ and $|V_B| < |V_{FB}|$ (the forward bias range). Since we focus on the *I-V* curve at 4 K ($k_BT = 0.35$ meV), the inelastic electron tunneling, the thermionic emission, and thermionic field emission through the barrier are excluded, namely, there is only the direct tunneling current. As shown below, the *I-V* curve of the Schottky barrier at $|V_B| < |V_{FB}|$ is helpful to estimate the donor doping concentration of the Si surface.

Figure 8(a) shows the *I-V* curve measured at 4 K for the Fe/Mg/MgO/n^+-Si junction with $d_{MgO} = 1.2$ nm and $t_{ox} = 0$ min, where the thin black and bold black curves represent the *I-V* curves in the forward and reverse bias ranges, respectively. Since the *I-V* curve does not show a rectifying feature, the direct tunneling occurs even when the magnitude of V_B is small in both the forward and reverse bias ranges [25]. As previously described, the Si surface is depleted when $V_B < 0$ and $|V_B| < |V_{FB}|$ (the forward bias range), as shown in Fig. 6(b). When $0 < |V_B| < |V_{FB}|$, the depletion layer width W_D in Fig. 7(b) becomes thicker and the barrier height $e\phi_S$ becomes smaller with increasing $|V_B|$. Using Eq. (4) in Ref. [30], the direct tunneling occurs in $0 < |V_B| < |V_{FB}|$ at 4 K when the surface doping concentration N_D' is higher than 6×10^{19} cm^{-3}. If $N_D' = 6 \times 10^{19}$ cm^{-3} (this is the lower limit, thus the worst case), using the relation $\rho_s(\Omega\text{cm}) = 0.00055 \times (N_D')^{-2/3}$ for bulk Si materials [29], the surface resistivity ρ_s increases by a factor of 1.2 compared with the resistivity of the Si substrate estimated by the van der Pauw method. In our estimation of P_S using Eqs. (1) and (2) at a certain ΔV_0^N, P_S is inversely proportional to $(\rho_s)^{0.5}$.

Thus, if $N_D{}'$ is $6 \times 10^{19}\,\mathrm{cm}^{-3}$ instead of $8 \times 10^{19}\,\mathrm{cm}^{-3}$, P_S is overestimated, and the calibrated spin polarization is $P_S \div 1.10$ using the increased ρ_s.

For $d_{MgO} = 1.2\,\mathrm{nm}$ and $t_{ox} = 1$ and 3 min, we obtained similar *I-V* curves which do not show a rectifying feature, as shown in Fig. 8(b). These results mean that the direct tunneling occurs in $0 < |V_B| < |V_{FB}|(V_B < 0)$. Thus, it is a reasonable conclusion that the doping concentration of the Si surface does not change for $t_{ox} = 0$, 1, and 3 min. Thus, the calibrated spin polarization is $P_S \div 1.10$ in all the t_{ox} cases, if $N_D{}' = 6 \times 10^{19}\,\mathrm{cm}^{-3}$.

D. Possibility of the change in the phosphorus doping concentration during the thermal oxidation

We describe another possibility of the change in the phosphorus donor doping concentration N_D during the thermal oxidation with dry O_2 gas at the initial stage of the device process. We found that the N_D value within 1200 nm from the Si surface can be larger than that of the Si substrate estimated from the van der Pauw method. Consequently, the resistivity $\rho_s(\Omega\mathrm{cm})$ near the Si surface becomes lower. In this case, P_S is underestimated and the calibrated spin polarization is $P_S \times 1.09$ using the decreased ρ_s.

The doping profile of donor atoms can change during the thermal oxidation, and it depends on donor atoms (phosphorus, arsenic, and antimony) and oxidation temperature. This doping profile change originates from the diffusion constants and the solubility of donor atoms in SiO_2 and Si. As a result, phosphorus atoms can pile up, which leads to the increase in N_D near the SiO_2/Si interface by thermal oxidation. From Ref. [31], when the oxidation is carried out at 1050 °C (this is our case), N_D increases by a factor of 1.2 and the diffusion length $2(Dt)^{0.5}$ is 1200 nm, where D and t represent the diffusion constant of phosphorus atoms in Si and the thermal oxidation time (60 min in our case), respectively. Based on this estimation, the initial doping concentration $N_D = 8 \times 10^{19}\,\mathrm{cm}^{-3}$ increases to $9.6 \times 10^{19}\,\mathrm{cm}^{-3}$. Unlike the very small band-bending width near the surface by the application of a positive bias voltage, the depth where N_D increases is comparable to the spin diffusion length $\lambda_S = \sim 1300\,\mathrm{nm}$. Thus, this increase in N_D near the Si surface probably has an influence on the estimation of P_S. Due to this increase in N_D, the resistivity ρ_s decreases by a factor of 1.1, which was estimated by the relation $\rho_s = 0.00055 \times (N_D{}')^{-2/3}$ [29]. In our estimation of P_S using Eqs. (1) and (2) at a certain ΔV_0^N, P_S is inversely proportional to $(\rho_s)^{0.5}$. Thus, in this case, P_S is underestimated and the calibrated spin polarization is $P_S \times 1.09$ using the decreased ρ_s.

E. Summary of our analysis

Our spin extraction signals were measured in the forward bias range ($V_B < 0, I_B < 0$) for the Schottky barrier near the Si surface (a high positive bias voltage is applied to the top Al pad, and the bias current I_B is negative). In this condition, the electronic band of Si is not depleted, but almost flat. Therefore, the resistivity of the Si surface is almost the same as that of the substrate, which was measured by the van der Pauw method. Thus, the P_S values estimated here are nearly accurate and reliable.

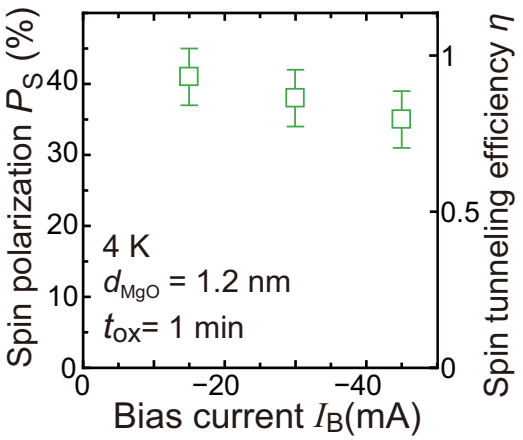

FIG. 9. Bias current I_B dependence of the spin polarization of tunneling electrons P_S measured for the sample with $d_{MgO} = 1.2\,\mathrm{nm}$ and $t_{ox} = 1\,\mathrm{min}$, where squares are the estimated P_S values [the same values as those in Fig. 5(c)] and a bar attached to each square is the possible range from the analysis of the surface phosphorus concentration N_D by the *I-V* curve of the junction and the redistribution of N_D during the thermal oxidation.

Furthermore, we have analyzed the possible nonuniform distribution of the phosphorus doping concentration N_D in Si near the surface, and suggested the possibility that P_S can be underestimated. Figure 9 shows the bias current $I_B(< 0)$ dependence of P_S for the sample with $t_{MgO} = 1.2\,\mathrm{nm}$ and $t_{ox} = 1\,\mathrm{min}$, in which the squares are the P_S values in Fig. 5(c) and a bar attached to each square represents the possible range due to the nonuniform distribution in electron carriers and N_D in Si near the surface. The upper limit in the range is P_S (square values) $\times$ 1.09, whereas the lower limit in the range is P_S (square values) $\div$ 1.10. From these results, the P_S values estimated here are nearly accurate and reliable. Thus, we concluded that the maximum P_S value obtained in our study is comparable to the spin polarization of Fe ∼44% .

In our device process, the thermal oxidation at the initial stage can increase N_D near the surface, but there is no reasonable origin to decrease N_D. Thus, there is a possibility that the true P_S values are the values of the upper limit in the ranges shown by the bars in Fig. 9, due to the increase in N_D near the surface by the thermal oxidation.

VI. CONCLUSION

We achieved a high η value of 0.93 by lowering the interface trap density D_{it} at the MgO/Si interface with inserting an ultrathin SiO_x layer, even when the MgO tunnel barrier layer is amorphous. Our result directly provides the evidence that electron spins are flipped by the interface traps at the MgO/Si interface when they are passing through the Fe/Mg/MgO/n^+-Si junction. Although this spin-flip mechanism has been anticipated by many researchers, here we experimentally demonstrate it with systematic and quantitative analyses of the interface traps.

To obtain higher magnetoresistance in devices with spin injector/extractor junctions and a Si channel, the conductivity matching between the junctions and channel is needed. Owing to the high RA, our junction does not meet the matching condition and thus a low magnetoresistance ratio is anticipated when the junctions are used as the spin injector/extractor. However, the significance of this study is that we have clarified the physics concerning spin injection/extraction by the strong evidence for spin flips at the tunnel barrier layer/Si interface. Our demonstration of high η by lowering D_{it} will be a useful guideline to develop the technology of spin injectors/extractors with ferromagnet/tunnel barrier/Si junctions.

ACKNOWLEDGMENTS

This work was partially supported by Grants-in-Aid for Scientific Research (Grant No. 16H02095), CREST of JST (Grant No. JPMJCR1777), Yazaki Memorial Foundation for Science and Technology, and Spintronics Research Network of Japan.

[1] S. Sugahara and M. Tanaka, Appl. Phys. Lett. **84**, 2307 (2004).
[2] S. Sugahara and M. Tanaka, ACM Trans. Storage **2**, 197 (2006).
[3] M. Tanaka and S. Sugahara, IEEE Trans. Electron Devices **54**, 961(2007).
[4] I. Appelbaum, B. Huang, and D. J. Monsma, Nature (London) **447**, 295 (2007).
[5] O. M. J. van't Erve, A. T. Hanbicki, M. Holub, C. H. Li, C. Awo-Affouda, P. E. Thompson, and B. T. Jonker, Appl. Phys. Lett. **91**, 212109 (2007).
[6] Y. Aoki, M. Kameno, Y. Ando, E. Shikoh, Y. Suzuki, T. Shinjo, M. Shiraishi, T. Sasaki, T. Oikawa, and T. Suzuki, Phys. Rev. B **86**, 081201 (2012).
[7] T. Tahara, H. Koike, M. Kameno, S. Sasaki, Y. Ando, K. Tanaka, S. Miwa, Y. Suzuki, and M. Shiraishi, Appl. Phys. Express **8**, 113004 (2015).
[8] M. Ishikawa, H. Sugiyama, T. Inokuchi, T. Tanamoto, K. Hamaya, N. Tezuka, and Y. Saito, J. Appl. Phys. **114**, 243904 (2013).
[9] A. Tiwari, T. Inokuchi, M. Ishikawa, H. Sugiyama, N. Tezuka, and Y. Saito, Jpn. J. Appl. Phys. **56**, 04CD05 (2017).
[10] S. Sato, R. Nakane, T. Hada, and M. Tanaka, Phys. Rev. B **96**, 235204 (2017); **97**, 199901 (2018).
[11] R. Nakane, T. Hada, S. Sato, and M. Tanaka, Appl. Phys. Lett. **112**, 182404 (2018).
[12] R. Wang, X. Jiang, R. M. Shelby, R. M. Macfarlane, S. S. P. Parkin, S. R. Bank, and J. S. Harris, Appl. Phys. Lett. **86**, 052901 (2005).
[13] X. Jiang, R. Wang, R. M. Shelby, R. M. Macfarlane, S. R. Bank, J. S. Harris, and S. S. P. Parkin, Phys. Rev. Lett. **94**, 056601 (2005).
[14] G. Schmidt, D. Ferrand, L. W. Molenkamp, A. T. Filip, and B. J. van Wees, Phys. Rev. B **62**, 4790(R) (2000).
[15] A. Fert and H. Jaffrès, Phys. Rev. B **64**, 184420 (2001).
[16] P. M. Tedrow and R. Meservey, Phys. Rev. B **7**, 318 (1973).
[17] S. Sato, R. Nakane, and M. Tanaka, Appl. Phys. Lett. **107**, 032407 (2015).
[18] R. Jansen, S. P. Dash, S. Sharma, and B. C. Min, Semicond. Sci. Technol. **27**, 083001 (2012), and references therein.
[19] R. Zhang, T. Iwasaki, N. Taoka, M. Takenaka, and S. Takagi, IEEE Trans. Electron Devices **59**, 335 (2012).
[20] F. J. Himpsel, F. R. McFeely, A. Taleb-Ibrahimi, J. A. Yarmoff, and G. Hollinger, Phys. Rev. B **38**, 6084 (1988).
[21] T. Aratani, M. Higuchi, S. Sugawa, E. Ikenaga, J. Ushio, H. Nohira, T. Suwa, A. Teramoto, T. Ohmi, and T. Hattori, J. Appl. Phys. **104**, 114112 (2008).
[22] See Supplemental Material at http://link.aps.org/supplemental/10.1103/PhysRevMaterials.3.024411 for (S1) subtraction of the background signal from the experimental three-terminal Hanle signal to obtain ΔV^{N}, (S2) supporting results indicating that the electronic band structure near the surface is not depleted, (S3) effect of the roughness-induced stray field on the spin polarization P_S estimated from the narrower Hanle signals, and (S4) estimation of D_{it} using the conductance method.
[23] Y. Song and H. Dery, Phys. Rev. Lett. **113**, 047205 (2014).
[24] E. H. Nicolian and J. R. Brews, *MOS Physics and Technology* (Wiley, New York, 1982).
[25] E. H. Rhoderick, *Metal-Semiconductor Contacts* (Oxford University press, UK, 1978).
[26] Y. Taur and T. K. Ning, *Fundamentals of Modern VLSI Devices* (Cambridge University Press, New York, 1998), Chap. 2, p. 66.
[27] J. Wagner and J. A. del Alamo, J. Appl. Phys. **63**, 425 (1988).
[28] M. I. Vexler, Solid-State Electron. **47**, 1283 (2003).
[29] F. Mousty, P. Ostoja, and L. Passari, J. Appl. Phys. **45**, 4576 (1974).
[30] Y. C. Yu, Solid-State Electron. **13**, 239 (1970).
[31] A.S. Groove, *Physics and Technology of Semiconductor Devices* (Wiley, New York, 1967), Chap. 3.5, pp. 69–75.